Magnetotransport of SrIrO₃-based heterostructures

A. K. Jaiswal, R. Schneider, M. Le Tacon, et al.

COLLECTIONS

Paper published as part of the special topic on 15th Joint MMM-Intermag Conference

View Online   Export Citation   CrossMark

ARTICLES YOU MAY BE INTERESTED IN

Optically pumped deep-UV multimode lasing in AlGaN double heterostructure grown by molecular beam homoepitaxy
AIP Advances **12**, 035023 (2022); https://doi.org/10.1063/5.0085365

Enhanced force-field calibration via machine learning
Applied Physics Reviews **7**, 041404 (2020); https://doi.org/10.1063/5.0019105

Machine learning for materials design and discovery
Journal of Applied Physics **129**, 070401 (2021); https://doi.org/10.1063/5.0043300

AIP Advances

Call For Papers!

SPECIAL TOPIC: Advances in Low Dimensional and 2D Materials

Magnetotransport of SrIrO₃-based heterostructures

A. K. Jaiswal,[a)] R. Schneider, M. Le Tacon, and D. Fuchs[a)] (ID)

AFFILIATIONS

Karlsruhe Institute of Technology, Institute for Quantum Materials and Technologies, 76021 Karlsruhe, Germany

Note: This paper was presented at the 15th Joint MMM-Intermag Conference.
[a)]Authors to whom correspondence should be addressed: arun.jaiswal@kit.edu and dirk.fuchs@kit.edu

ABSTRACT

Transition-metal oxide (TMO) based heterostructures provide fertile playground to explore or functionalize novel quantum materials. In this regard, the combination of $3d$ and $5d$ TMOs have gained special interest because of the simultaneous appearance of strong spin–orbit coupling and electron correlation at the interface of those heterostructures. Artificial breaking of the inversion symmetry in heterostructures may also result in a distinct interfacial Dzyaloshinskii-Moriya interaction (DMI) and the formation of non-collinear magnetic spin structures in case of magnetic TMOs. Among the $5d$ TMOs, SrIrO₃ (SIO) has gained significant attention because of its large spin–orbit coupling and the semi-metallic ground state, which are highly susceptible to structural distortions. Here, we report on the preparation and the characterisation of structural, electronic and magnetic properties of epitaxial heterostructures consisting of the $5d$ TMO SIO and the $3d$ antiferromagnetic insulator LaFeO₃.

I. INTRODUCTION

Transition-metal oxide (TMO) based heterostructures (HS) and interfaces offer a unique way to engineer novel quantum states that are absent in the bulk counterparts of their constituting materials.[1] In addition, the complex interplay between lattice, orbit, charge and spin degree of freedom provides an opportunity to design specific properties and functionalities that could for instance serve as basis for the next-generation spintronic devices.[2] A well-known example is the interface between the two non-magnetic band insulators LaAlO₃ and SrTiO₃, where a conducting and possibly magnetic two-dimensional electron gas (2DEG) has been observed. This interface has shown a large, electrically tuneable spin-to-charge conversion.[3] Apart from these 2DEGs, heterostructures comprising $4d$- and $5d$- TMOs with strong spin–orbit coupling also present a promising platform for new quantum states.[4]

Among the $5d$ TMOs, SrIrO₃ (SIO) is of current interest.[5] It shows large spin–orbit coupling and a semi-metallic ground state that is highly susceptible to structural distortions.[6–8] However, the electron correlation in $5d$ TMOs is usually too small to host ferromagnetism. Recently, ultra-thin SIO films and superlattices (SL)

with thickness less than 4-unit cells have shown structurally induced metal to insulator- and magnetic phase transitions demonstrating the correlation between structural and electric/magnetic properties.[9] In SIO, a magnetic ground state should be achievable by tuning the competition between Coulomb interaction and spin–orbit coupling.[10] The effect of magnetic substrate on the magnetotransport properties of SIO has also been demonstrated, where a hysteretic magnetoresistance at 2K was observed.[11]

Recently, SIO based HSs and SLs have demonstrated interesting properties. In particular, iridate-manganite (La₁₋ₓSrₓMnO₃ (LSMO)-SIO)) HSs and SLs have shown interfacial charge transfer from iridate to the manganite layer which leads to the formation of molecular orbitals at the interface.[12–14] Indications of a ferromagnetic ground state of SIO were deduced from x-ray magnetic circular dichroism (XMCD).[12,14] Skoropata et al. have also reported on a topological Hall effect in SIO/LSMO SLs which has been discussed in the context of skyrmion-like magnetic textures at the interface.[13,15,16]

Here, we report on the synthesis and the characterisation of high-quality heterostructures, where we have combined SIO with a $3d$ antiferromagnetic insulator LaFeO₃ (LFO). Bulk LFO is a G-type antiferromagnetic insulator with one of the largest known

Neel temperature T_N = 740 K.[17,18] It shows a large magnetic moment of 3.8-4.0 μ_B/Fe.[19,20] The combination of $3d$ and $5d$ TMOs provides competition between spin–orbit coupling and electron correlation at the interface and is thus expected to be a promising route to generate magnetic exchange across the interface producing a magnetic ground state in SIO. A clear observation of anomalous Hall effect and butterfly shaped magnetoresistance suggest a proximity induced magnetic state in SIO.

II. EXPERIMENTAL

SIO and LFO thin films were deposited by pulsed laser deposition using a KrF excimer laser. The films were deposited from stoichiometric homemade polycrystalline targets on TiO_2-terminated $SrTiO_3$ (STO) (001) substrates. Surface termination was carried out by standard buffered HF etch and high temperature annealing. A clear step-terrace like surface structure with a step height of one STO unit cell was observed by atomic force microscopy. During the growth, substrate temperature and laser frequency was kept fixed at 700 °C and 2 Hz, respectively. For the LFO films, we used a laser energy of $E \approx 2$ mJ/cm^2 and an oxygen partial pressure of $P(O_2)$ = 5 × 10^{-5} mbar, and for SIO $E \approx 1$ mJ/cm^2 and $P(O_2)$ = 0.1 mbar. The heterostructures were capped with a 5 nm thick STO capping layer to protect the layers from any possible degradation. Film thickness of the individual layers were controlled by *in situ* reflection high energy electron diffraction (RHEED). After the deposition, samples were *in situ* post-annealed in 500 mbar oxygen pressure for 30 minutes to reduce possible oxygen deficiencies. Structural properties were characterized by X-ray reflectivity and diffraction using a Bruker D8 Davinci diffractometer.

Magnetic properties of the HS were recorded with a superconducting quantum interference device (SQUID). Magnetization data were corrected with respect to the diamagnetic background from the STO substrate.

To analyse electrical transport, contacts to the HS were made with a wire bonder using aluminium wire in Van der Pauw geometry. The measurements were carried out with a physical property measurement system (PPMS). Magnetoresistance and Hall data were symmetrized and anti-symmetrized, respectively.

III. RESULTS AND DISCUSSION

Fig. 1(a) shows the x-ray reflectivity (XRR) and x-ray diffraction (XRD) of the LFO and SIO single layers and the SIO/LFO bilayer. The film thicknesses were determined by simulating the XRR data. The thicknesses are 17nm, 22nm and 22/17 nm for the LFO, SIO and SIO/LFO samples, respectively. The right panel in Fig. 1(a) show the XRD of the samples in the vicinity of the pseudo-cubic (001) and (002) reflections. Clear thickness oscillations are observed in the diffraction which reflects the high degree of crystallinity of the samples. The out-of-plane lattice parameters for LFO and SIO films were determined from the peak positions and are nearly the same, i.e., 4.0 Å. The HS also shows no distinct splitting of the film peaks so that same out of plane lattice parameters for SIO and LFO in the HS can be assumed as well.

In Fig. 1(b), we show the resistivity ρ versus T of the SIO single layer and SIO/LFO HS. Both show qualitatively similar behavior, i.e., ρ decreases with decreasing T until a minimum is reached at
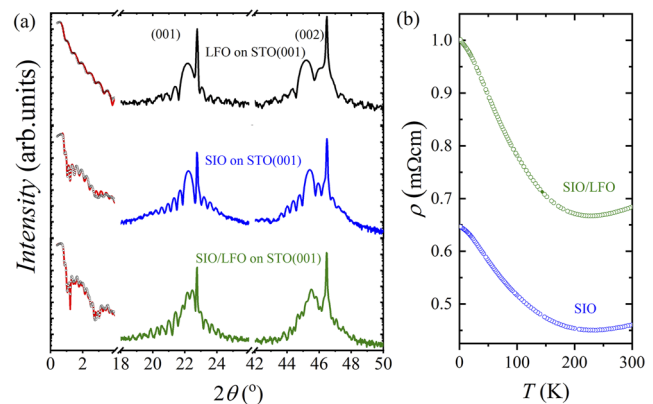

FIG. 1. (a) X-ray reflectivity and x-ray diffraction of LFO, SIO and SIO/LFO grown on TiO$_2$- STO (001) substrate. Intensity is plotted on logarithmic scale. The black circles represent the measured XRR data and red solid lines are the corresponding fits to the XRR data. Diffraction is shown for the pseudo-cubic (001) and (002) reflection. (b) Resistivity ρ versus T for SIO and SIO/LFO heterostructure.

$T_{min} \approx 220$ K. For T < T_{min}, ρ increases with decreasing T. This is also consistent with other reports and indicates the semi-metallic nature of SIO.[13,21,22] Note, that the resistivity of the HS is larger compared to that of the SIO single layer which is likely related to a lower charge carrier concentration as indicated by Hall measurements. Due to the insulating behavior of LFO, it does not contribute to the conductivity of the HS.

Next, we report on the magnetotransport properties of SIO/LFO HS. Fig. 2(a) shows the magnetoresistance (*MR*) of SIO/LFO at 2K with applied magnetic field perpendicular to the film surface. A small hysteretic butterfly shaped *MR* is observed at low temperatures which suggests towards the possible magnetic state in the SIO. Usually, hysteretic behavior of MR originates from magnetic domains in a ferromagnetic metal. For instance, a similar hysteretic *MR* has been observed at 2K in SIO films on DyScO$_3$ (110) substrate,[11] induced by the magnetic DyScO$_3$. In Fig. 2(b), we show the Hall resistance (R_{xy}) versus magnetic field at 2 K. Apart from the linear ordinary Hall resistance (OHR), an additional hysteretic contribution to R_{xy} is observed, see inset Fig. 2(b). In the context of magnetism, the contribution is known as the anomalous Hall resistance R_{xy}^{AHE} (AHR)[23] which can be extracted by subtracting the linear part from the measured R_{xy}. Generally, in ferromagnetic metals the magnetic scattering of charge carries result in a butterfly shaped hysteretic magnetotransport behavior (*MR* ~ −M^2 and R_{xy}^{AHE} ~ M). This is indeed the case here. The Magnetoresistance at low temperatures show a clear butterfly shaped hysteretic MR, which suggests a magnetic state in SIO at the interface. The magnetic state is again confirmed from the observation of a hysteretic anomalous Hall resistance. Fig. 2(c) shows the ordinary Hall resistance R_{xy}^{OHE} of the SIO/LFO HS. R_{xy}^{OHE} is linear and the negative slope documents the dominating electron like transport behavior which is usually observed for SIO films on STO. Assuming a one-type charge carrier transport, the charge carrier concentration n amounts to about 3.0 × 10^{20} cm^{-3} and 4.6 × 10^{20} cm^{-3} at 10 K for SIO/LFO HS and SIO, respectively. The low carrier concentration in the SIO/LFO HS hints toward a possible charge transfer from SIO to LFO, which
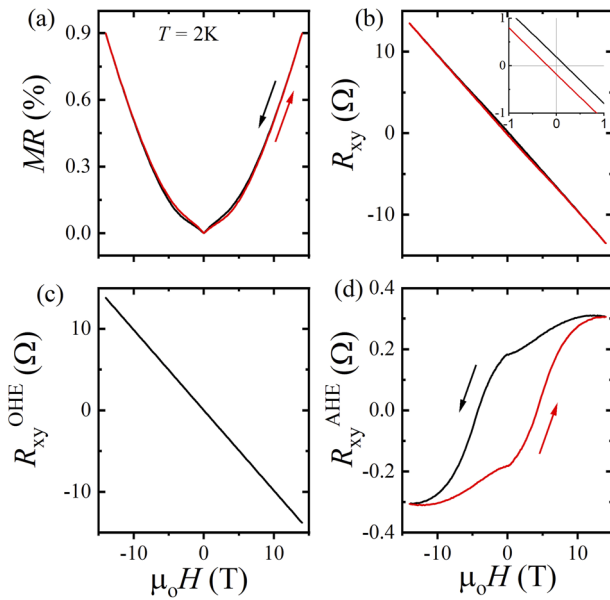
FIG. 2. Magnetotransport of SIO/LFO HS at T = 2K. (a) Magnetoresistance (MR) vs. field ($\mu_o H$) at 2 K. Arrows and color indicate the field sweep directions. (b) The Hall resistance (R_{xy}) vs. $\mu_o H$. Inset: R_{xy} at low fields where a hysteretic behavior can be observed. (c) Ordinary part of the Hall resistance vs. $\mu_o H$. (d) Anomalous part of the Hall resistance vs. $\mu_o H$. Arrows and color indicate the field sweep directions.

FIG. 3. (a) Anomalous Hall resistance vs. $\mu_o H$ for a SIO/LFO HS at various temperatures. (b) The maximum value $\langle R_{xy}^{AHE} \rangle$ of the AHR (at $\mu_o H$ = 14 T) vs. T.

FIG. 4. (a) Magnetic moment m^* versus $\mu_o H$ for the SIO/LFO HS at various temperatures. The linear diamagnetic contribution from the substrate has been subtracted from the measured data. (b) Normalized anomalous Hall resistance and magnetic moment of SIO/LFO HS vs. $\mu_o H$ at T = 10K.

has been observed in SIO/LSMO. In Fig. 2(d), we show the extracted AHR of the SIO/LFO HS. The AHR is positive and opposite to what have been observed in LSMO-SIO heterostructures.[12,13] The sign of anomalous Hall resistance is directly related to the Berry curvature (BC) and so to the electronic band structure at the Fermi energy. To give a definite answer on the sign of the AHR calculations of the BC are needed. The coercive field is rather large and similar to the coercive field observed in MR. Usually, AHE is considered as a signature of magnetic polarization.[23] Since the transport is limited to SIO, the observed AHR is also related to the SIO layer only and indicates induced magnetism in SIO.

Fig. 3(a) shows the extracted AHR for different temperatures. The AHR displays very large coercivity field below 10 K, where a full saturation is obviously not achieved even for 14 T. An additional hump like feature can be seen at 2 K. This might be related to some anisotropic behavior of the sample caused by the non-saturated magnetization and a failure of the van der Pauw measurement in case of inhomogeneous sample magnetization.

Fig. 3(b) shows the maximum value $\langle R_{xy}^{AHE} \rangle$ of the AHR at 14 T versus T. The $\langle R_{xy}^{AHE} \rangle$ decreases with increasing temperature and becomes almost zero at room temperature. Since the R_{xy}^{AHE} is usually proportional to the magnetization ($R_{xy}^{AHE} \sim M$[23]), the T-dependence of R_{xy}^{AHE} suggests an onset of magnetism in SIO.

Magnetization measurements of the SIO/LFO HS are reported in Fig. 4. In Fig. 4(a), the magnetic moment m^* is shown versus $\mu_o H$ at different temperatures which compares well to that of single LFO films (not shown here). The diamagnetic signal from the STO substrate has been removed by subtracting the linear part of
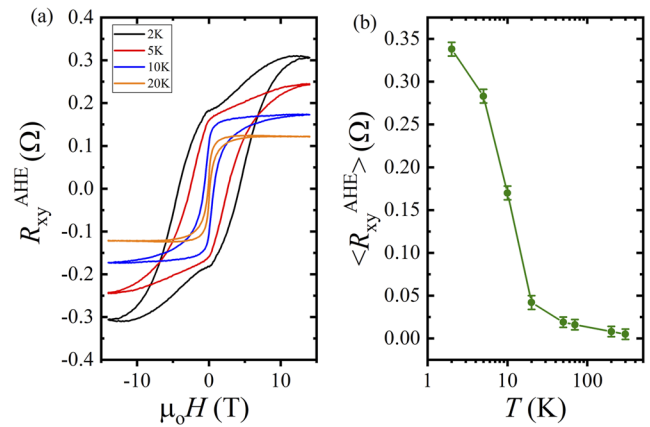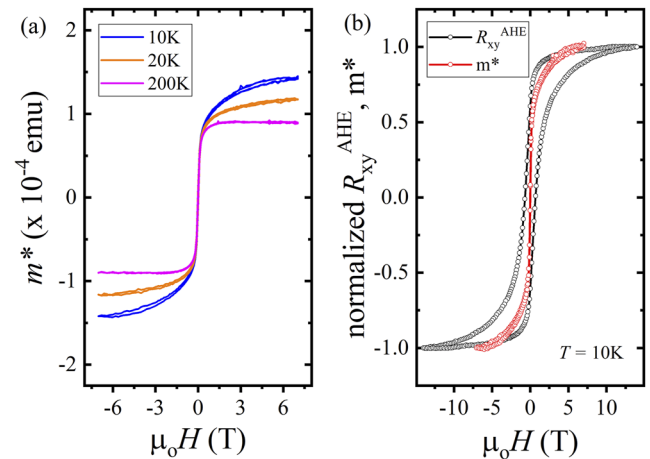
m^* vs $\mu_o H$, which has been determined at $\mu_o H > 6$ T. m^* vs. $\mu_o H$ shows a hysteretic behavior with a small coercive field H_c around 200 Oe at 10K. The magnetic moments arise from the Fe^{+3} in LFO. The estimated moment from the magnetization measurements is about 2.2 μ_B/Fe which is half of the observed moments in bulk LFO.[19,20] The saturation magnetization decreases with increasing temperature.

Fig. 4(b) displays the normalized R_{xy}^{AHE} and m^* of the SIO/LFO HS at 10K. They both show a very different coercive field. Since, the magnetic moment of the HS is dominated by the LFO signal, the large coercivity of the AHE cannot be due to the magnetization of LFO but again indicates the relation to SIO. As the induced magnetism in SIO is supposed to be limited to the interfacial region of the SIO layer the contribution to m^* is expected to

be very small, which makes a direct measurement by SQUID very difficult. However, decreasing the layer thickness of LFO and SIO in corresponding HSs and SLs will facilitate the characterization of the magnetic state in SIO.

IV. SUMMARY AND CONCLUSIONS

In conclusion, high quality epitaxial SIO/LFO heterostructures were grown by pulsed laser deposition. Clear observation of an anomalous Hall resistance and a butterfly shaped hysteretic magnetoresistance indicates magnetism in the heterostructures related to SIO. The similar coercivity of MR and R_{xy}^{AHE} consistently demonstrates the presence of a ferromagnetic state in SIO. The presented results show the possibility to induce magnetism in $5d$ TMOs close to room temperature and hence the importance of $3d - 5d$ TMO interfaces for the exploration of new magnetic states where both strong spin–orbit coupling and electron correlation can be included.

ACKNOWLEDGMENTS

AUTHOR DECLARATIONS

Conflict of Interest

The authors have no conflicts to disclose.

DATA AVAILABILITY

The data that support the findings of this study are available from the corresponding authors upon reasonable request.

REFERENCES

[1] H. Y. Hwang, Y. Iwasa, M. Kawasaki, B. Keimer, N. Nagaosa, and Y. Tokura, Nat. Mater. **11**, 103 (2012).

[2] D. C. Vaz, A. Barthélémy, and M. Bibes, Jpn. J. Appl. Phys. **57**, 0902A4 (2018).

[3] E. Lesne, Y. Fu, S. Oyarzun, J. C. Rojas-Sánchez, D. C. Vaz, H. Naganuma, G. Sicoli, J.-P. Attané, M. Jamet, E. Jacquet, J.-M. George, A. Barthélémy, H. Jaffrès, A. Fert, M. Bibes, and L. Vila, Nat. Mater. **15**, 1261 (2016).

[4] H. Chen and D. Yi, APL Mater. **9**, 060908 (2021).

[5] L. Zhang (n. d.).

[6] Y. F. Nie, P. D. C. King, C. H. Kim, M. Uchida, H. I. Wei, B. D. Faeth, J. P. Ruf, J. P. C. Ruff, L. Xie, X. Pan, C. J. Fennie, D. G. Schlom, and K. M. Shen, Phys. Rev. Lett. **114**, 016401 (2015).

[7] A. Biswas, K. S. Kim, and Y. H. Jeong, J. Appl. Phys. **116**, 213704 (2014).

[8] N. Manca, D. J. Groenendijk, I. Pallecchi, C. Autieri, L. M. K. Tang, F. Telesio, G. Mattoni, A. Mccollam, S. Picozzi, and A. D. Caviglia, Phys. Rev. B **97**, 081105 (2018).

[9] P. Schütz, D. Di Sante, L. Dudy, J. Gabel, M. Stübinger, M. Kamp, Y. Huang, M. Capone, M. A. Husanu, V. N. Strocov, G. Sangiovanni, M. Sing, and R. Claessen, Phys. Rev. Lett. **119**, 256404 (2017).

[10] M. A. Zeb and H.-Y. Kee, Phys. Rev. B **86**, 085149 (2012).

[11] A. K. Jaiswal, A. G. Zaitsev, R. Singh, R. Schneider, and D. Fuchs, AIP Adv. **9**, 125034 (2019).

[12] J. Nichols, X. Gao, S. Lee, T. L. Meyer, J. W. Freeland, V. Lauter, D. Yi, J. Liu, D. Haskel, J. R. Petrie, E. Guo, A. Herklotz, D. Lee, T. Z. Ward, G. Eres, M. R. Fitzsimmons, and H. N. Lee, Nat. Commun. **7**, 12721 (2016).

[13] E. Skoropata, J. Nichols, J. M. Ok, R. V. Chopdeka, E. S. Choi, A. Rastogi, C. Sohn, X. Gao, S. Yoon, T. Farmer, R. D. TDesautel, D. Haskel, J. W. Freelan, S. Okamoto, M. Brahlek, and H. N. Lee, Sci. Adv. **6**, eaaz3902 (2020).

[14] M. W. Yoo, J. Tornos, A. Sander, L. F. Lin, N. Mohanta, A. Peralta, D. Sanchez-Manzano, F. Gallego, D. Haskel, J. W. Freeland, D. J. Keavney, Y. Choi, J. Strempfer, X. Wang, M. Cabero, H. B. Vasili, M. Valvidares, G. Sanchez-Santolino, J. M. Gonzalez-Calbet, A. Rivera, C. Leon, S. Rosenkranz, M. Bibes, A. Barthelemy, A. Anane, E. Dagotto, S. Okamoto, S. G. E. te Velthuis, J. Santamaria, and J. E. Villegas, Nat. Commun. **12**, 3283 (2021).

[15] N. Mohanta, E. Dagotto, and S. Okamoto, Phys. Rev. B **100**, 064429 (2019).

[16] Y. Li, L. Zhang, Q. Zhang, C. Li, T. Yang, Y. Deng, L. Gu, and D. Wu, ACS Appl. Mater. Interfaces **11**, 21268 (2019).

[17] M. Eibschütz, S. Shtrikman, and D. Treves, Phys. Rev. **156**, 562 (1967).

[18] J. E. Kleibeuker, Z. Zhong, H. Nishikawa, J. Gabel, A. Müller, F. Pfaff, M. Sing, K. Held, R. Claessen, G. Koster, and G. Rijnders, Phys. Rev. Lett. **113**, 237402 (2014).

[19] M. A. Ahmed and S. I. El-Dek, Mater. Sci. Eng. B Solid-State Mater. Adv. Technol. **128**, 30 (2006).

[20] X. D. Zhou, Q. Cai, J. Yang, M. Kim, W. B. Yelon, W. J. James, Y. W. Shin, B. J. Scarfino, and H. U. Anderson, J. Appl. Phys. **97**, 10C314 (2005).

[21] K. R. Kleindienst, K. Wolff, J. Schubert, R. Schneider, and D. Fuchs, Phys. Rev. B **98**, 115113 (2018).

[22] A. K. Jaiswal, R. Schneider, R. Singh, and D. Fuchs, Appl. Phys. Lett. **115**, 031904 (2019).

[23] N. Nagaosa, J. Sinova, S. Onoda, A. H. MacDonald, and N. P. Ong, Rev. Mod. Phys. **82**, 1539 (2010).